

# Charge-Density-Wave Transitions of Dirac Fermions Coupled to Phonons

Chuang Chen,<sup>1,2</sup> Xiao Yan Xu,<sup>3</sup> Zi Yang Meng,<sup>1,4</sup> and Martin Hohenadler<sup>5</sup>

<sup>1</sup>*Beijing National Laboratory for Condensed Matter Physics and Institute of Physics,  
Chinese Academy of Sciences, Beijing 100190, China*

<sup>2</sup>*School of Physical Sciences, University of Chinese Academy of Sciences, Beijing 100190, China*

<sup>3</sup>*Department of Physics, Hong Kong University of Science and Technology, Clear Water Bay, Hong Kong, China*

<sup>4</sup>*CAS Center of Excellence in Topological Quantum Computation and School of Physical Sciences,  
University of Chinese Academy of Sciences, Beijing 100190, China*

<sup>5</sup>*Institut für Theoretische Physik und Astrophysik, Universität Würzburg, 97074 Würzburg, Germany*

(Dated: December 15, 2024)

The spontaneous generation of charge-density-wave order in a Dirac fermion system via the natural mechanism of electron-phonon coupling is studied in the framework of the Holstein model on the honeycomb lattice. Using two independent and unbiased quantum Monte Carlo methods, the phase diagram as a function of temperature and coupling strength is determined. It features a quantum critical point as well as a line of thermal critical points. Finite-size scaling appears consistent with fermionic Gross-Neveu-Ising universality for the quantum phase transition, and bosonic Ising universality for the thermal phase transition. The critical temperature has a maximum at intermediate couplings. Our findings motivate experimental efforts to identify or engineer Dirac systems with sufficiently strong and tunable electron-phonon coupling.

The experimental advances in preparing single-layer graphene [1] have put Dirac fermions at the focus of condensed matter physics. While the single-electron properties are relatively well understood, correlation effects remain a highly active area of research [2]. Due to the two-dimensional (2D) nature of the problem, theoretical models can be analyzed by powerful theoretical and numerical methods, offering the prospect of a comprehensive understanding. The field has recently received another boost by the remarkable properties of other honeycomb systems, in particular quantum spin-Hall physics in bismuthene [3] and unconventional superconductivity in twisted bilayer graphene [4]. Finally, massive Dirac phases such as charge-density-wave (CDW) insulators in transition-metal dichalcogenides [5] promise future applications in optoelectronics.

Theoretical studies of massive 2+1D Dirac fermions were pioneered by Semenoff [6], who considered a staggered fermion density or CDW, and Haldane [7], who introduced a topological mass that produces an integer quantum Hall state in the absence of a magnetic field. Such problems become even richer if the masses arise from spontaneous symmetry breaking at interaction-driven phase transitions. Particularly remarkable aspects of Dirac systems are that (i) phase transitions occur at nonzero critical values and (ii) the gapless fermionic excitations can strongly modify the critical behavior, giving rise to fermionic quantum critical points [8–17]. The interplay of different order parameters provides a route to deconfined quantum critical points [18] and emergent symmetries [19, 20], see Ref. [21] for a review.

Numerous interactions have been explored numerically in the framework of honeycomb lattice models. A sufficiently strong onsite Hubbard repulsion yields an antiferromagnetic Mott insulator [22–24]. The same holds

for a more realistic  $1/r$  Coulomb repulsion, although the nonlocal part of the interaction—relevant for graphene where screening is absent—enhances CDW fluctuations [25]. A dominant nearest-neighbor repulsion favors a CDW state [26–30] but is rather unrealistic; for spinful fermions, quantum Monte Carlo (QMC) simulations are hampered by the sign problem. Mean-field predictions of interaction-generated topological states in extended Hubbard models [26] inspired significant efforts to address fluctuation effects. For spinless fermions, unbiased numerical methods reveal the absence of topological phases but support CDW, valence bond solid, and charge-modulated ground states (see Ref. [31] for a review). Similar conclusions were recently reached for the spinful problem [32, 33]. Finally, bond-bond interactions were found to produce valence bond, antiferromagnetic, quantum spin-Hall, and CDW states [12, 14, 34].

Here, we consider electron-phonon coupling as the mechanism for CDW order. QMC investigations along these lines have so far been restricted by the challenges in simulating electron-phonon models, as addressed by several recent methodological advances [35–38]. We carried out large-scale QMC simulations of the fundamental Holstein molecular-crystal model [39] to determine the phase diagram as a function of coupling strength and temperature. Moreover, we investigate the nature of the observed quantum and thermal phase transitions.

*Model.*—Within the Holstein model, electrons coupled to quantum phonons on the honeycomb lattice are described by the Hamiltonian

$$\hat{H} = -t \sum_{\langle ij \rangle \sigma} \hat{c}_{i\sigma}^\dagger \hat{c}_{j\sigma} + \sum_i \left[ \frac{1}{2M} \hat{P}_i^2 + \frac{\kappa}{2} \hat{Q}_i^2 \right] - g \sum_i \hat{Q}_i \hat{\rho}_i. \quad (1)$$

The first term represents nearest-neighbor electronic hop-

ping, the second term Einstein phonons at each lattice site, and the third term the coupling between fluctuations of the local electron number  $\hat{\rho}_i = \hat{n}_i - 1$  and the lattice displacement  $\hat{Q}_i$ . Here,  $\hat{n}_i = \sum_{\sigma} \hat{c}_{i\sigma}^\dagger \hat{c}_{i\sigma}$ , the phonon frequency  $\omega_0 = \sqrt{\kappa/M}$ , and we introduce the dimensionless coupling  $\lambda = g^2/(\kappa W)$  with the free bandwidth  $W = 6t$ . We consider half-filling and work in units where  $k_B$ ,  $\hbar$  and the lattice constant are equal to one.

For  $\lambda = 0$ , Eq. (1) gives the well-known semimetallic band structure  $\epsilon(\mathbf{k})$  with linear excitations at the Dirac points  $K, K'$  [1]. An expansion around these points yields a Dirac equation in terms of eight-component spinor fields corresponding to  $N = 2$  (spin  $\uparrow, \downarrow$ ) Dirac fermions with two flavors (valleys  $K, K'$ ) and two pseudospin directions (sublattices A,B) [1].

*Methods.*—We used the determinant QMC (DQMC) method [40] and the continuous-time interaction expansion (CT-INT) QMC method [41]. In the former case, the electrons are integrated out and the phonons are sampled using local and block updates [42, 43] as well as global moves based on an effective bosonic model determined by self-learning [36, 44, 45]. In CT-INT, the phonons are integrated out and the resulting electronic model with a retarded interaction is sampled [46]. While CT-INT works in continuous imaginary time, a Trotter discretization  $\Delta\tau = 0.1$  was used for DQMC. Although both methods are in principle capable of simulating any parameters, CT-INT is most efficient at weak coupling and less problematic with respect to autocorrelations [35]. DQMC requires more care regarding the sampling but—especially in combination with self-learning—can access stronger couplings and larger system sizes. We used lattices with  $L \times L$  unit cells ( $2L^2$  sites) and  $L = 3n$  ( $n = 1, 2, \dots$ ) whose reciprocal lattice contains the Dirac points that determine the low-energy physics.

*Phase diagram.*—The existence of CDW order at sufficiently strong coupling can be inferred from two opposite limits. For classical phonons ( $\omega_0 = 0$ ), we can make a mean-field ansatz  $\hat{Q}_i \mapsto (-1)^i \bar{Q}$ , corresponding to a staggered chemical potential or Semenoff mass that breaks the sublattice and chiral symmetry [6]. The lattice displacements are accompanied by a density imbalance  $\delta = |\langle \hat{n}^A \rangle - \langle \hat{n}^B \rangle|$  (see inset of Fig. 1). The band structure acquires a gap at the Fermi level,  $E(\mathbf{k}) = \pm \sqrt{\epsilon^2(\mathbf{k}) + \Delta^2}$ . Spontaneous mass generation is described by a gap equation identical to that for the Mott transition of the Hubbard model upon identifying  $\bar{Q} = m/2$  ( $\Delta = g\bar{Q}$ ),  $\lambda W = U$ . The mean-field critical value is  $U_c = 2.23t$  or  $\lambda_c = 0.37$  [22], which may be compared to  $U_c \approx 3.8t$  or  $\lambda_c \approx 0.63$  from QMC [23, 24, 47]. The nonzero critical value reflects the stability of the semimetal at weak coupling [8], the origin of which is the linearly vanishing density of states,  $N(\omega) \sim |\omega|$  [1].

In the opposite, antiadiabatic limit  $\omega_0 \rightarrow \infty$ , integrating out the phonons in the path-integral representation yields an attractive Hubbard model with  $U = \lambda W$  [48].

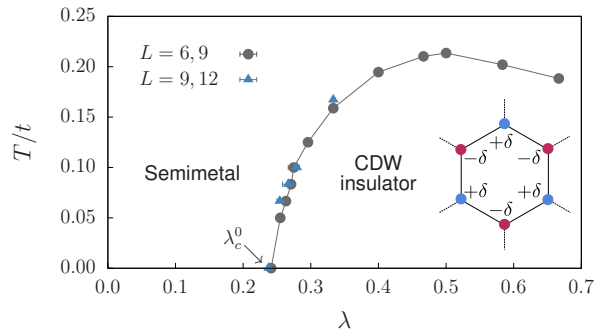


FIG. 1. Phase diagram of the Holstein model on the honeycomb lattice for  $\omega_0 = 0.5t$ . CDW order with a staggered charge disproportionation  $\pm\delta$  (inset) exists beyond a quantum critical point at  $\lambda_c^0 \approx 0.2375$  and below a critical temperature  $T_c(\lambda)$ . The critical values were obtained from the crossings of the correlation ratio  $R_c$  for different system sizes  $L$  using CT-INT ( $T \leq 0.05t$ ) and DQMC ( $T > 0.05t$ ), respectively.

By symmetry [49],  $U_c$  has the same magnitude as for the Mott transition of the repulsive Hubbard model, namely  $3.8t$  [23, 24, 47]. The Hubbard model has a higher symmetry than the Holstein model [48], which leads to a combined  $SO(3)$  order parameter for CDW and superconducting order at  $U > U_c$  and  $T = 0$  [50]. A mean-field decoupling with an Ising order parameter—reflecting the two possible choices for the sign of the excess charge  $\delta$  in Fig. 1—gives again  $U_c = 2.23t$  or  $\lambda_c = 0.37$ .

For quantitative insights into the experimentally relevant case of finite  $\omega_0$ , we turn to QMC simulations. We focus on  $\omega_0 = 0.5t$ , for which both quantum fluctuations and retardation effects are significant. We determined critical values either at fixed coupling or at fixed temperature. The values reported in Fig. 1 are based on the renormalization-group invariant correlation ratio  $R_c = 1 - S_c(\mathbf{Q} + \delta\mathbf{q})/S_c(\mathbf{Q})$  [51] calculated from the charge structure factor  $S_c(\mathbf{q}) = L^{-2} \sum_{ij} e^{-i\mathbf{q} \cdot (\mathbf{r}_i - \mathbf{r}_j)} \langle (\hat{n}_i^A - \hat{n}_i^B)(\hat{n}_j^A - \hat{n}_j^B) \rangle$ . The CDW order is within the unit cell, so the ordering wavevector  $\mathbf{Q} = \Gamma = (0, 0)$ . If  $\mathbf{Q} + \delta\mathbf{q}$  is a neighboring point in the Brillouin zone, long-range order and hence a divergence of  $S_c(\Gamma)$  implies  $R_c \rightarrow 1$  for  $L \rightarrow \infty$ , otherwise  $R_c \rightarrow 0$ . At the critical point,  $R_c$  is independent of  $L$  up to scaling corrections, so that the critical value can be estimated from intersections of  $R_c$  for different  $L$ . Crucially, the scaling holds independent of any critical exponents and  $R_c$  usually has smaller scaling corrections than  $S_c(\Gamma)$  [51, 52].

To detect the quantum critical point, we take  $\beta t = L$  based on the expected emergent Lorentz symmetry [53]. Figure 2(a) suggests a critical value  $\lambda_c^0 \approx 0.2375$ . Similar analysis for other parameters yields the phase boundary in Fig. 1, shown in terms of the intersections of  $L = 6, 9$  and  $L = 9, 12$ , respectively. Apart from the absence of long-range order at  $\lambda < \lambda_c^0$  [Fig. 2(a)], the CDW transition is also apparent in the single-particle spectral func-

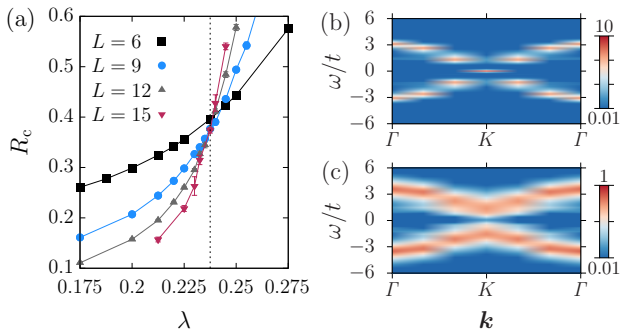


FIG. 2. (a) Estimation of the critical value  $\lambda_c^0 \approx 0.2375$  for the quantum critical point from the intersections of the correlation ratio  $R_c$ . Here,  $\beta t = L$ ,  $\omega_0 = 0.5t$ . Single-particle spectral function  $A(\mathbf{k}, \omega)$  in (b) the semimetallic phase ( $\lambda = 0.1$ ) and (c) the CDW phase ( $\lambda = 0.4$ ) for  $\beta t = L = 9$ . Results were obtained with the CT-INT method.

tion  $A(\mathbf{k}, \omega)$  [54]. We find gapless excitations at the Dirac point for  $\lambda = 0.1$  [Fig. 2(b)] and a gap at the Fermi level for  $\lambda = 0.4$  [Fig. 2(c)].

In Fig. 1, CDW order persists up to a critical temperature  $T_c$ . After an initial increase, asymptotically determined by the quantum critical point via  $T_c \sim |\lambda - \lambda_c^0|^{z\nu}$  [30],  $T_c$  takes on a maximum before decreasing at even stronger couplings [55]. This can be understood within an effective  $t$ - $V$  model of singlet bipolarons (hardcore bosons) [48]. Although the bipolaron energy continues to grow with  $\lambda$ , the exchange interaction  $V$  that sets the temperature for CDW order in this regime ( $T_c \sim J$  for the Ising model) decreases. An expression for  $V$  in the Holstein model is given in Ref. [48] and simplifies to  $V \sim t/\lambda$  for  $\omega_0 \gg t$ . The decrease of  $T_c$  with increasing interaction strength  $\lambda$  contrasts  $T_c \sim V$  in models for CDW order from Coulomb repulsion [30, 56, 57]. Finally, the phase boundary is expected to shift to stronger couplings at larger  $\omega_0$  due to enhanced lattice fluctuations, reaching  $\lambda_c^0 \approx 0.63$  [23, 24, 47] in the Hubbard limit  $\omega_0 \rightarrow \infty$  where  $T_c \equiv 0$  for any  $\lambda > \lambda_c^0$  due to the continuous  $\text{SO}(3)$  symmetry.

*Quantum phase transition.*—In Dirac systems, the Yukawa coupling between the gapless fermions and order parameter fluctuations described by Gross-Neveu field theories gives rise to fermionic critical points rather than Wilson-Fisher bosonic critical points [8, 9]. Gross-Neveu-Ising universality for CDW transitions was previously observed for  $N = 1$  Dirac fermions with nearest-neighbor Coulomb repulsion [27–30], and  $N = 2$  Dirac fermions with bond interactions [14, 34]. For the Holstein model, Gross-Neveu-Heisenberg universality is well established [24, 47, 58] for  $\omega_0 \rightarrow \infty$ , where it maps to the attractive Hubbard model. The 3+1D Gross-Neveu theory for the adiabatic limit  $\omega_0 \rightarrow 0$  should have a correlation length exponent  $\nu = 1/2$  [24]. For general  $\omega_0$ , 2+1D,  $N = 2$  Gross-Neveu-Ising universality is expected.

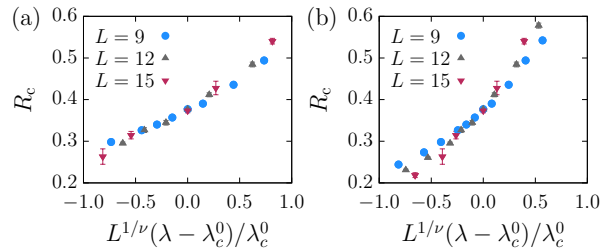


FIG. 3. Scaling collapse of the correlation ratio  $R_c$  using  $\lambda_c^0 = 0.2375$  and (a)  $1/\nu = 1.2$ , (b)  $1/\nu = 0.931$ .

For a preliminary analysis, we use  $\lambda_c^0 = 0.2375$  from Fig. 2(a) and available estimates for the exponent  $\nu$  from QMC simulations ( $1/\nu = 1.2(1)$  [34]) and the  $\epsilon$ -expansion ( $1/\nu = 0.931$  [59]), respectively. The rescaled correlation ratio for  $L = 9, 12, 15$  in Fig. 3 appears more consistent with  $1/\nu = 1.2$  [Fig. 3(a)] than with  $1/\nu = 0.931$  [Fig. 3(b)]. As a further consistency check, we determined  $\lambda_c^0$  from the best scaling collapse [60] on the interval  $[-1, 1]$ . The exponent  $1/\nu = 0.931$  yields  $\lambda_c^0 \approx 0.2489(3)$ , whereas  $1/\nu = 1.2$  yields  $\lambda_c^0 \approx 0.240(1)$ , closer to the estimate from Fig. 2(a) that was obtained without any assumption about the value of  $\nu$ .

A direct estimate of  $\nu$  based on an improved data set appears feasible and is motivated by the rather different existing estimates [59]. At the same time, a potential additional complication—absent in fermionic models—is that the phonon frequency interpolates between three different fixed points, namely mean-field scaling ( $\nu = 1/2$  [24]) at  $\omega_0 = 0$ , Gross-Neveu-Ising scaling for  $\omega_0 > 0$ , and Gross-Neveu-Heisenberg scaling for  $\omega_0 = \infty$ . For  $\omega_0 = 0.5t$ , the proximity to the adiabatic fixed point may give rise to crossover effects in the exponents. Another interesting possibility that has to be ruled out is the formation of singlet pairs—triggered by the attractive component of the frequency-dependent fermion-fermion interaction—prior to the CDW transition, as in the 1D Holstein model [61]. In this case, we would expect a bosonic, 3D Ising transition. Both the expected  $\omega_0 = 0$  value ( $1/\nu = 2$  [24]) and the 3D Ising value ( $1/\nu \approx 1.59$  [62]) are larger than predicted for the  $N = 2$  Gross-Neveu-Ising universality class [59].

*Thermal phase transition.*—Starting from the CDW ground state at  $\lambda > \lambda_c^0$ , long-range order is destroyed by thermal fluctuations at  $T_c$ . The phase transition is expected to exhibit 2D Ising universality with critical exponents  $\beta = 1/8$  and  $\nu = 1$ . Figure 4(a) shows that for  $\omega_0 = 0.5t$  and  $\lambda = 1/3$ , the rescaled charge structure factor has a crossing of different system sizes consistent with  $T_c = 0.159(2)$  in Fig. 1. The best scaling collapse on the interval  $[-2, 2]$  shown in Fig. 4(b) yields  $T_c = 0.1607(1)t$ , again in agreement with Fig. 1.

*Discussion.*—Our investigation of spontaneously generated CDW order from electron-phonon coupling on the

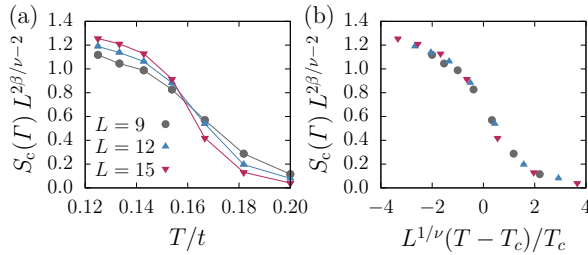


FIG. 4. Finite-size scaling of the density structure factor using the 2D Ising critical exponents  $\beta = 1/8$ ,  $\nu = 1$ . The critical temperature  $T_c = 0.162t$  was obtained from the best scaling collapse shown in (b). Here,  $\omega_0 = 0.5t$ ,  $\lambda = 1/3$ . Results obtained with the DQMC method.

honeycomb lattice reveals several differences to previous work. Perhaps most importantly, the Dirac band structure gives rise to a quantum critical point with expected Gross-Neveu-Ising universality at nonzero coupling. In contrast, the Fermi liquid of the square lattice is expected to have a weak-coupling instability due to perfect nesting and a Van Hove singularity [35, 63]. The thermal CDW transition appears to have the same Ising universality as for the square lattice [35–37, 64]. Such a transition is absent in the antiadiabatic limit, corresponding to the attractive Hubbard model. While the latter is useful to describe superconductivity away from half-filling, it supports long-range CDW order only at  $T = 0$  [50]. Models with dominant nearest-neighbor repulsion capture the finite-temperature CDW transition [30, 56, 57] but not the suppression of  $T_c$  at strong coupling.

**Outlook.**—There are several interesting future directions. The fermionic quantum criticality requires additional efforts. Superconductivity at nonzero doping and the competition between CDW order and antiferromagnetism in a Holstein-Hubbard model should be investigated. Our work may also provide a starting point for more realistic modeling of twisted bilayer graphene [4] or transition-metal dichalcogenides [5]. On the experimental side, a key question is if CDW order from electron-phonon coupling can be realized in one of the many Dirac systems currently being investigated.

We thank F. Assaad and I. Herbut for helpful discussions. MH acknowledges support by the DFG through SFB 1170 ToCoTronics; CC and ZYM by the Ministry of Science and Technology of China through the National Key Research and Development Program (grant 2016YFA0300502), the Strategic Priority Research Program of the Chinese Academy of Sciences (XDB28000000), and the National Science Foundation of China (11574359); XYX by HKRGC (C6026-16W, 16324216, 16307117). We thank the John von Neumann Institute for Computing (NIC) for computer resources on JURECA [65] at the Jülich Supercomputing Centre (JSC), the Center for Quantum Simulation Sciences at

Institute of Physics, Chinese Academy of Sciences, and the Tianhe-1A platform at the National Supercomputer Center in Tianjin for technical support and generous allocation of CPU time.

- 
- [1] A. H. C. Neto, F. Guinea, N. M. R. Peres, K. S. Novoselov, and A. K. Geim, *Rev. Mod. Phys.* **81**, 109 (2009).
  - [2] H.-K. Tang, J. Leaw, J. Rodrigues, I. Herbut, P. Sengupta, F. Assaad, and S. Adam, *Science* **361**, 570 (2018).
  - [3] F. Reis, G. Li, L. Dudy, M. Bauernfeind, S. Glass, W. Hanke, R. Thomale, J. Schäfer, and R. Claessen, *Science* **357**, 287 (2017).
  - [4] Y. Cao, V. Fatemi, S. Fang, K. Watanabe, T. Taniguchi, E. Kaxiras, and P. Jarillo-Herrero, *Nature* **556**, 43 (2018).
  - [5] S. Manzeli, D. Ovchinnikov, D. Pasquier, O. V. Yazyev, and A. Kis, *Nat. Rev. Materials* **2**, 17033 (2017).
  - [6] G. W. Semenoff, *Phys. Rev. Lett.* **53**, 2449 (1984).
  - [7] F. D. M. Haldane, *Phys. Rev. Lett.* **61**, 2015 (1988).
  - [8] I. F. Herbut, *Phys. Rev. Lett.* **97**, 146401 (2006).
  - [9] I. F. Herbut, V. Juričić, and O. Vafek, *Phys. Rev. B* **80**, 075432 (2009).
  - [10] M. M. Scherer and I. F. Herbut, *Phys. Rev. B* **94**, 205136 (2016).
  - [11] Z. Zhou, D. Wang, Z. Y. Meng, Y. Wang, and C. Wu, *Phys. Rev. B* **93**, 245157 (2016).
  - [12] Z.-X. Li, Y.-F. Jiang, S.-K. Jian, and H. Yao, *Nature Comm.* **8**, 314 (2017).
  - [13] L. Classen, I. F. Herbut, and M. M. Scherer, *Phys. Rev. B* **96**, 115132 (2017).
  - [14] Y.-Y. He, X. Y. Xu, K. Sun, F. F. Assaad, Z. Y. Meng, and Z.-Y. Lu, *Phys. Rev. B* **97**, 081110 (2018).
  - [15] E. Torres, L. Classen, I. F. Herbut, and M. M. Scherer, *Phys. Rev. B* **97**, 125137 (2018).
  - [16] X. Y. Xu, K. T. Law, and P. A. Lee, *Phys. Rev. B* **98**, 121406 (2018).
  - [17] T. C. Lang and A. M. Läuchli, *arXiv preprint arXiv:1808.01230* (2018).
  - [18] T. Senthil, A. Vishwanath, L. Balents, S. Sachdev, and M. P. A. Fisher, *Science* **303**, 1490 (2004).
  - [19] T. Sato, M. Hohenadler, and F. F. Assaad, *Phys. Rev. Lett.* **119**, 197203 (2017).
  - [20] Y. Q. Qin, Y.-Y. He, Y.-Z. You, Z.-Y. Lu, A. Sen, A. W. Sandvik, C. Xu, and Z. Y. Meng, *Phys. Rev. X* **7**, 031052 (2017).
  - [21] C. Wang, A. Nahum, M. A. Metlitski, C. Xu, and T. Senthil, *Phys. Rev. X* **7**, 031051 (2017).
  - [22] S. Sorella and E. Tosatti, *Europhys. Lett.* **19**, 699 (1992).
  - [23] S. Sorella, Y. Otsuka, and S. Yunoki, *Sci. Rep.* **2**, 992 (2012).
  - [24] F. F. Assaad and I. F. Herbut, *Phys. Rev. X* **3**, 031010 (2013).
  - [25] M. Hohenadler, F. Parisen Toldin, I. F. Herbut, and F. F. Assaad, *Phys. Rev. B* **90**, 085146 (2014).
  - [26] S. Raghu, X.-L. Qi, C. Honerkamp, and S.-C. Zhang, *Phys. Rev. Lett.* **100**, 156401 (2008).
  - [27] E. F. Huffman and S. Chandrasekharan, *Phys. Rev. B* **89**, 111101 (2014).
  - [28] L. Wang, P. Corboz, and M. Troyer, *New J. Phys.* **16**,

- 103008 (2014).
- [29] Z.-X. Li, Y.-F. Jiang, and H. Yao, *New J. Phys.* **17**, 085003 (2015).
  - [30] S. Hesselmann and S. Wessel, *Phys. Rev. B* **93**, 155157 (2016).
  - [31] S. Capponi, *J. Phys.: Condens. Matter* **29**, 043002 (2016).
  - [32] D. S. de la Peña, J. Lichtenstein, and C. Honerkamp, *Phys. Rev. B* **95**, 085143 (2017).
  - [33] M. Bijelic, R. Kaneko, C. Gros, and R. Valentí, *Phys. Rev. B* **97**, 125142 (2018).
  - [34] S. Chandrasekharan and A. Li, *Phys. Rev. D* **88**, 021701 (2013).
  - [35] M. Weber and M. Hohenadler, *Phys. Rev. B* **98**, 085405 (2018).
  - [36] C. Chen, X. Y. Xu, J. Liu, G. Batrouni, R. Scalettar, and Z. Y. Meng, *Phys. Rev. B* **98**, 041102 (2018).
  - [37] G. G. Batrouni and R. T. Scalettar, *arXiv:1808.08973* (2018).
  - [38] S. Karakuzu, K. Seki, and S. Sorella, *arXiv:1808.07759* (2018).
  - [39] T. Holstein, *Ann. Phys. (N.Y.)* **8**, 325 (1959); **8**, 343 (1959).
  - [40] R. Blankenbecler, D. J. Scalapino, and R. L. Sugar, *Phys. Rev. D* **24**, 2278 (1981).
  - [41] A. N. Rubtsov, V. V. Savkin, and A. I. Lichtenstein, *Phys. Rev. B* **72**, 035122 (2005).
  - [42] R. T. Scalettar, R. M. Noack, and R. R. P. Singh, *Phys. Rev. B* **44**, 10502 (1991).
  - [43] S. Johnston, E. A. Nowadnick, Y. F. Kung, B. Moritz, R. T. Scalettar, and T. P. Devereaux, *Phys. Rev. B* **87**, 235133 (2013).
  - [44] J. Liu, Y. Qi, Z. Y. Meng, and L. Fu, *Phys. Rev. B* **95**, 041101 (2017).
  - [45] X. Y. Xu, Y. Qi, J. Liu, L. Fu, and Z. Y. Meng, *Phys. Rev. B* **96**, 041119 (2017).
  - [46] F. F. Assaad and T. C. Lang, *Phys. Rev. B* **76**, 035116 (2007).
  - [47] F. Parisen Toldin, M. Hohenadler, F. F. Assaad, and I. F. Herbut, *Phys. Rev. B* **91**, 165108 (2015).
  - [48] J. E. Hirsch and E. Fradkin, *Phys. Rev. B* **27**, 4302 (1983).
  - [49] C. N. Yang and S. Zhang, *Mod. Phys. Lett. B* **4**, 759 (1990).
  - [50] J. E. Hirsch, *Phys. Rev. B* **31**, 4403 (1985).
  - [51] K. Binder, *Z. Phys. B Con. Mat.* **43**, 119 (1981).
  - [52] S. Pujari, T. C. Lang, G. Murthy, and R. K. Kaul, *Phys. Rev. Lett.* **117**, 086404 (2016).
  - [53] I. F. Herbut, V. Juričić, and B. Roy, *Phys. Rev. B* **79**, 085116 (2009).
  - [54] We applied the stochastic maximum entropy [66] implementation of ALF [67] to the imaginary-time Green function traced over the sublattices and averaged over spin.
  - [55] S. Blawid and A. J. Millis, *Phys. Rev. B* **63**, 115114 (2001).
  - [56] J. E. Gubernatis, D. J. Scalapino, R. L. Sugar, and W. D. Toussaint, *Phys. Rev. B* **32**, 103 (1985).
  - [57] M. Bercx, J. S. Hofmann, F. F. Assaad, and T. C. Lang, *Phys. Rev. B* **95**, 035108 (2017).
  - [58] Y. Otsuka, S. Yunoki, and S. Sorella, *Phys. Rev. X* **6**, 011029 (2016).
  - [59] N. Zerf, L. N. Mihaila, P. Marquard, I. F. Herbut, and M. M. Scherer, *Phys. Rev. D* **96**, 096010 (2017).
  - [60] O. Melchert, *arXiv:0910.5403* (2009).
  - [61] M. Hohenadler and F. F. Assaad, *Phys. Rev. B* **87**, 075149 (2013).
  - [62] M. Hasenbusch, K. Pinn, and S. Vinti, *Phys. Rev. B* **59**, 11471 (1999).
  - [63] F. Marsiglio, *Phys. Rev. B* **42**, 2416 (1990).
  - [64] N. C. Costa, T. Blommel, W.-T. Chiu, G. Batrouni, and R. T. Scalettar, *Phys. Rev. Lett.* **120**, 187003 (2018).
  - [65] Jülich Supercomputing Centre (2016), in *JURECA: General-purpose supercomputer at Jülich Supercomputing Centre*, Journal of Large-Scale Research Facilities, Vol. 2, p. A62, <http://dx.doi.org/10.17815/jlsrf-2-121>.
  - [66] K. S. D. Beach, *arXiv:cond-mat/0403055* (2004).
  - [67] M. Bercx, F. Goth, J. S. Hofmann, and F. F. Assaad, *SciPost* **3**, 013 (2017).